THE ASTROPHYSICAL JOURNAL, 463:535–542, 1996 June 1

LOW SURFACE BRIGHTNESS GALAXIES IN THE LOCAL UNIVERSE. II. SELECTION EFFECTS AND COMPLETENESS OF THE AUTOMATED PLATE MEASURING[1] SURVEY

D. SPRAYBERRY
Kapteyn Laboratorium, Postbus 800, NL-9700 AV Groningen, The Netherlands; dspray@astro.rug.nl
C. D. IMPEY
Steward Observatory, University of Arizona, Tucson, AZ 85721; cimpey@as.arizona.edu
AND
M. J. IRWIN
Royal Greenwich Observatory, Madingley Road, Cambridge CB3 0EZ, UK; mike@mail.ast.cam.ac.uk
Received 1995 July 21; accepted 1995 December 5

ABSTRACT

We discuss the techniques employed for identifying low surface brightness galaxies for the Automated Plate Measuring (APM) survey. We present the method of calibrating the photometry performed from the APM scans and discuss the uncertainties associated with the calibrations. We also review the possible sources of incompleteness in the survey, and we present the results of a program of simulations to estimate the completeness as a function of galaxy parameters. Finally, we discuss the implications of the survey results and show, in particular, that the observed distribution of central surface brightnesses among all galaxies in one survey field is almost flat for $\mu_B(0) > 23$ mag arcsec^{-2}.

Subject headings: galaxies: photometry — methods: data analysis — surveys

1. INTRODUCTION

Surface brightness selection bias can severely affect our understanding of the local galaxy population. Impey et al. (1996) present a list of low surface brightness (LSB) galaxies previously uncataloged because of this bias. This paper describes the methods used to develop the list of galaxies presented by Impey et al. (1996) and analyzes the selection effects inherent in those methods.

One approach to locating a population of LSB galaxies uses observational techniques with much fainter limiting isophotes than is conventional with standard Schmidt telescope survey plates, such as amplified photographs (e.g., Impey, Bothun, & Malin 1988), matched detection filters optimized for finding large low surface brightness objects (e.g., Irwin et al. 1990), which are equivalent in performance to amplified photographs, or CCD surveys (e.g., Davies et al. 1994). These techniques can sample a relatively large range of the surface brightness distribution (whatever it may be), but at present they have only been applied to modest regions of sky. The other approach is to examine normal Schmidt telescope survey plates *very* carefully. This does not provide the extremely faint limiting isophotes available from other techniques but does make wide-field surveys possible. Schombert & Bothun (1988) and Schombert et al. (1992) have developed a list of over 300 LSB galaxies by visually searching plates from the second Palomar Observatory Sky Survey. The analysis of galaxies from their lists (e.g., McGaugh & Bothun 1994) has provided valuable insight into the properties of LSB galaxies, but the impossibility of judging the completeness of visual surveys has limited the statistical use of them.

We have also adopted the technique of careful examination of existing survey plates, but we have chosen to combine visual searches with automated scanning. The use of automated scanning allows the completeness of the resulting galaxy list to be estimated objectively, thus making the survey results useful for statistical analyses such as the estimation of a luminosity function. In this paper, we discuss the process of identifying LSB galaxies from UK Schmidt Telescope (UKST) survey plates (§ 2) and describe the photometric calibrations that make possible magnitude estimates of the identified galaxies (§ 3). We also analyze the completeness of the resulting galaxy list and obtain, through simulations, an objective estimate of the survey completeness as a function of galaxy parameters (§ 4). Finally, we discuss the implications of our survey results for the question of whether there exists a typical value of central surface brightness for spiral galaxies (§ 5). The list of LSB galaxies and a summary of the follow-up observations are contained in Impey et al. (1996). Future papers will address such issues as the luminosity function of the LSB galaxies from this survey, the bivariate luminosity–surface brightness distribution, and the bivariate luminosity–H I mass distribution.

2. THE SELECTION PROCESS

Target LSB galaxies were identified using a combination of both automated and eyeball searches of glass copies of UKST IIIa-J survey plates. Twenty-four equatorial fields covering an area of 786 deg^2 of sky were surveyed, with the candidate LSB galaxies selected from a total of well over 10 million images in the strip.

The Automated Plate Measuring (APM) facility at Cambridge was used to locate all objects on a plate meeting certain criteria (for a general description of the APM facility, see Kibblewhite et al. 1984). To be included as a candidate LSB galaxy, an object must have a minimum area of 2.5 log $N = 6.5$, where N is the number of connected pixels at or above the detection threshold. The detection threshold is set at 2 σ above the modal value of the background, where σ is the pixel noise level of the background.

[1] The Automated Plate Measuring (APM) Facility is a National Astronomy Facility, at the Institute of Astronomy, operated by the Royal Greenwich Observatory.

This detection threshold corresponds to a typical surface brightness of $\mu_B = 24.5 \pm 0.5$ mag arcsec^{-2} as determined from the photometric calibrations described in § 3. The uncertainty in this number reflects both the uncertainty in the photometric calibration and the scatter from plate to plate. Images are defined as groups of contiguous pixels above the detection threshold. The plates were measured at a resolution of 15 μm, with a pixel sampling of 7.5 μm, or 0.″51 pixel^{-1}, given the 67.″14 mm^{-1} scale of the UKST plates. The minimum image area defined previously is thus $\approx$100 arcsec^2 on the sky. A radial exponential model was fitted to the unsaturated part of the areal profile (pixel intensity vs. number of pixels at that intensity), and a candidate object was also required to have an extrapolated model central surface brightness of $\mu_B(0) \gtrsim 22$ mag arcsec^{-2}. This second criterion eliminates virtually all of the so-called "normal" galaxies from the sample. The objects revealed by these scans were then reviewed by eye to eliminate as many previously cataloged galaxies, plate flaws, Galactic cirrus clouds, and other interlopers as possible. No records were kept of the number of objects rejected during this visual review. Finally, each detected object that passed the visual review was digitized in a raster scan of 512 × 512 pixels (for objects $\gtrsim$30″ in diameter) or 256 × 256 pixels (for objects $\lesssim$30″ in diameter).

The visual search was carried out independently of the automatic scan, using a combination of low power (×5) binocular microscope and direct eye search. A similar visual search in the Fornax cluster (Irwin et al. 1990) had shown that direct visual examination of UKST glass copy survey plates could detect LSB galaxies with central SB as low as 26 mag arcsec^{-2}, but that the success rate was a strong function of the image scale size and difficult to quantify. Each plate was searched in lanes ~5 cm wide, and any LSB feature or galaxy with unusual extended morphology was noted. Straightforward use of a 40 cm graduated rule sufficed to locate the candidates to within $\frac{1}{2}$ mm with respect to the plate edges. Knowledge of the plate center, scale, and orientation enabled these "x-y" coordinates to be translated into celestial coordinates with an accuracy of better than 1′. These celestial coordinates were sufficiently accurate that the images could then be automatically measured (in the form of two-dimensional pixel maps) using the APM. Subsequent centroiding from the two-dimensional maps enabled accurate (~1″) coordinates to be obtained. We note that both the visual and machine searches used glass copies rather than original UKST survey plates because (1) the background density is adjusted during copying to be roughly constant (~0.6D), irrespective of the original plate background density; (2) a modest amount of contrast enhancement around sky background is also folded in, which in conjunction with (1) makes LSB features easier to see; (3) exhaustive tests have shown that the information content of original plates is not noticeably degraded by good quality contact copying; and (4) the copy plates are readily available, and the originals are not.

Objects selected by eye are then combined with the machine-selected sample in a master list of candidates for follow-up CCD photometry, optical spectroscopy, and 21 cm radio observation. The eyeball search is a necessary adjunct to the automated scanning because the global parametric requirements of the automatic search cannot be guaranteed to pick out all galaxies of manifestly unusual morphology. The Malin 1 type galaxies (see Bothun et al. 1987 and Sprayberry et al. 1993) provide excellent illustrations of this problem. Galaxies with such prominent nuclei are not picked out by average surface brightness measures. Although, given the benefit of hindsight, it is possible to generalize the automatic selection criteria to cope with cases like this, eventually the selection criteria become too complicated to readily interpret in terms of easily measurable galactic properties, and there is no guarantee of picking all interesting types. It is more logical to rely on the machine search to ensure completeness to some simple well-defined selection boundaries and to use the visual search to include a wider variety of interesting morphologies.

This two-part process resulted in a final list of 693 target galaxies, of which 494 are previously uncataloged. Because of various practical constraints on the completion of the survey, the complete list was assembled from two components. The large angular size or "LAS" list included 513 galaxies that are generally $\gtrsim$30″ in diameter; the small angular size or "SAS" list covered the remaining 180 objects that are predominantly $\lesssim$30″ in diameter. The LAS list was completed first, and the galaxies on that list have much better morphological information available from the APM scans, so the galaxies targeted for follow-up observation were chosen from the LAS list.

3. PHOTOMETRIC CALIBRATION

Photometric calibration of the digitized APM scans was carried out using the general method outlined by Cawson et al. (1987). This method involves comparing the APM scans with externally calibrated CCD images of the same galaxies. As part of our campaign of follow-up observations, we obtained CCD photometry in Johnson B and V bands and Kron-Cousins R bands of 125 of the target objects. Galaxies were selected for CCD photometry based on several criteria. The most important of these criteria included covering a representative sample of the morphologies seen in the survey, covering as many of the 24 UKST plates as possible, and observational constraints such as minimizing air mass while maximizing observing efficiency. Nineteen nights of observations were carried out with the Steward Observatory 2.3 m telescope on Kitt Peak. The 19 nights were separated into eight observing runs over the period 1990 December–1992 September. Observations prior to 1992 May (about 80% of the total) used a thinned Texas Instruments (TI) 800 × 800 pixel detector, and those after 1992 May (the remaining 20%) used a thick Loral 2048 × 2048 pixel detector. Both detectors have 15 μm pixels, and both were used in direct imaging mode with 2 × 2 on-chip binning to yield an image scale of 0.″3 pixel^{-1}. Field size was 2′ × 2′ for the TI and 5′ × 5′ for the Loral. Bias subtraction, dark current subtraction, and flat-fielding were carried out with the IRAF[2] data reduction package. Standard stars from the lists of Christian et al. (1985) or Odewahn, Bryja, & Humphreys (1992) were used for photometric calibrations. At least two standard star fields were observed each night, giving an average of 15 stars per night. Internal errors in each night's photometric zero points were typically $\approx$0.03 mag, and the scatter among the zero points for each detector was $\approx$0.06 mag for the TI detector and $\approx$0.08 mag for the Loral detector.

[2] The Image Reduction and Analysis Facilities package is distributed by NOAO, which is operated by AURA, Inc., under contract to the National Science Foundation.

After eliminating galaxy images that were compromised by weather or instrumental problems, or by defects in the APM scans (e.g., the galaxy being too near the edge of the plate), 106 galaxies remained for use in calibrating the APM scans. The breakdown of calibrators in each field appears in Table 1. Magnitudes and $B-V$ and $V-R$ colors for these galaxies were measured by aperture photometry in circular apertures centered on the intensity peak of the galaxy. First, the sky background was measured and subtracted from the image. The backgrounds were measured by making histograms of the pixel values in the four corners of each image, or in other regions well away from the galaxy if the galaxy was not centered in the frame. A Gaussian was fit to the central peak of each histogram, and the center (the mode of the pixel histogram) and width of that Gaussian were adopted as the background level and its uncertainty in that region. Then, for each image, the four modal values were ranked, the highest and lowest discarded, and the average of the two remaining was taken to be the background for the entire image. Next, the appropriate aperture radius was determined by measuring the total intensity within expanding concentric apertures until the intensity versus radius growth curve became flat. Increasing the aperture radius in a number of small steps to determine the appropriate maximum also allowed a straightforward estimate of the half-light radius as the radius of the circular aperture that enclosed half of the total intensity found within the maximum aperture. Finally, a central surface intensity was determined by measuring the average intensity per pixel within the smallest concentric aperture. This smallest aperture had a diameter of 4″ to provide an adequate signal-to-noise ratio in the lowest surface brightness objects. The measured intensities were then converted to magnitudes and magnitudes per square arcsecond using zero points and color terms derived from the standard stars observed on that night, and the magnitudes and surface brightnesses were corrected for Galactic extinction using the reddening maps of Burstein & Heiles (1982). The k-corrections from the tabulations of Coleman, Wu, & Weedman (1980) were applied to all objects with measured velocities; the tabulated colors of their Sbc, Scd, and Irr types match the range of measured colors for the LSB galaxies nicely. The surface brightnesses and magnitudes of these objects were then corrected for cosmological dimming as $(1+z)^4$ and $(1+z)^2$, respectively. The magnitude corrections ranged from -0.004 to -0.27 with a mean of -0.06, and the surface brightness corrections ranged from -0.007 to -0.54 with a mean of -0.12. For most galaxies in the catalog, z is low enough that these corrections are unimportant, but since the corrections are necessary for some galaxies, they were applied uniformly to all.

TABLE 1

UKST Fields: Photometric Calibrations

Field Number (1)	R.A. (2)	TI (3)	Loral (4)	σ (5)
892	23:00	4	0	0.19
893	23:20	4	2	0.19
894	23:40	4	2	0.21
824	00:20	4	3	0.23
826	01:00	7	0	0.22
827	01:20	0	3	0.25
828	01:40	0	3	0.25
830	02:20	0	2	0.25
831	02:40	9	0	0.21
833	03:20	6	0	0.16
834	03:40	8	0	0.15
835	04:00	2	0	0.25
851	09:20	7	0	0.20
853	10:00	7	0	0.14
854	10:20	3	0	0.25
855	10:40	4	0	0.24
856	11:00	3	0	0.25
857	11:20	3	0	0.25
859	12:00	4	0	0.20
860	12:20	6	0	0.24
862	13:00	2	0	0.25
863	13:20	1	0	0.25
865	14:00	0	1	0.25
867	14:40	0	2	0.25

Note.—Col. (1) lists the UKST plate numbers. Col. (2) lists the center R.A.s as hh:mm (1950.0). Center decl. = 0 for all plates. Col. (3) lists the number of calibrator galaxies observed with the TI CCD. Col. (4) lists the number of calibrator galaxies observed with the Loral CCD. Col. (5) is the adopted uncertainty in the APM-to-CCD transformation in magnitudes.

Following the prescription of Cawson et al. (1987), we determined the transformation between APM "density" units and CCD intensities using the following seven steps. First, the CCD image was rebinned to the same pixel scale as the APM scan (0.″51 pixel^{-1}). Second, the CCD image and APM scan were registered using foreground stars present in both images, and both images were trimmed to the same size. Third, the backgrounds were measured as described above and subtracted from the CCD image and APM scan. Fourth, the background-subtracted CCD image was scaled from B to the B_J bandpass of the APM scans using the transformation $B_J = B - 0.25(B-V)$ (per Blair & Gilmore 1982) and the overall B magnitude and $B-V$ color of the galaxy previously determined from the CCD photometry. Fifth, the background-subtracted CCD image was divided by its exposure time, and the APM image was scaled by the ratio of APM units to UKST plate density units (10,000 APM units = 1 unit of plate density). Sixth, a scatter plot was formed between normalized CCD intensity and plate density for each pixel. This scatter plot has a clustering at the origin, since most pixels are sky. The ridgeline of this scatter plot defines the characteristic curve of the scanned plate section. Two examples appear in Figure 1. Finally, an average characteristic curve was determined for each UKST plate, and a fourth-order polynomial fit to that average curve is then used to transform the scaled APM values pixel by pixel into normalized CCD intensities, which can be calibrated into magnitudes using the standard-star zero points. The average characteristic curves for four representative plates appear in Figure 2, along with the overall average for the plates that had more than three calibrating galaxies.

The number of calibrator galaxies varies considerably from field to field. Also, characteristic curves determined from the Loral CCD are not usable in combination with those determined from the TI CCD, due to the differences in quantum efficiency and color response of the two detectors. While it would in principle be possible to combine individual curves from the two detectors by calibrating the vertical axes into physical flux units (e.g., ergs cm^{-2} s^{-1} over the filter bandpass), there is no practical reason for doing so with these data. Only three of our UKST fields have calibrator galaxies observed with both detectors, and all three are well calibrated by the galaxies observed with the TI

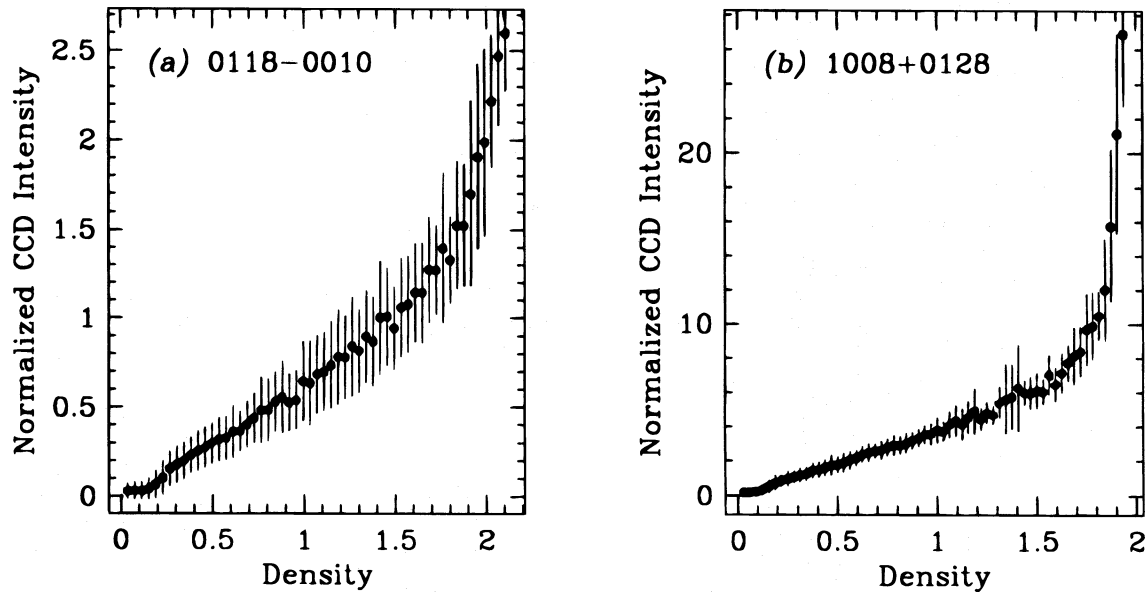

FIG. 1.—Examples of characteristic curves obtained from individual APM scans. Each point represents the average of all points from the scatter plot within a bin of width 0.05 units in normalized APM density. The vertical axis is in units of CCD intensity, normalized by the exposure time, and the horizontal axis is in units of UKST plate density. Galaxy 0118−0010 in (*a*) was observed with the Loral 2048 × 2048 CCD, and Galaxy 1008+0128 in (*b*) was observed with the TI 800 × 800 CCD. Note the difference between the vertical axis scalings due to the difference in *B*-band quantum efficiency between the two CCDs.

CCD. For both these reasons, we determined plate-average curves only for the 13 plates that have four or more calibrator galaxies observed with the same CCD. For these 13 plates, the uncertainties quoted in Table 1 are the formal uncertainties computed from the scatter among the calibrator galaxies for each plate. For the remaining 11 plates, we used the average of all the plate-average curves from the 13 well-calibrated plates. For these 11 plates, the quoted uncertainties reflect the external scatter among the transformations of the other 13 plates. This external scatter (0.25 mag) is about as large as the largest internal uncertainty (0.24 mag) for any one of the 13 well-calibrated plates. As a final external check, we estimated magnitudes for the 106 calibrator galaxies from their APM scans using these transformations. The mean magnitude difference $m_{CCD} - m_{APM}$ was -0.11 ± 0.26 (rms), which is consistent with the transformation uncertainties quoted in Table 1.

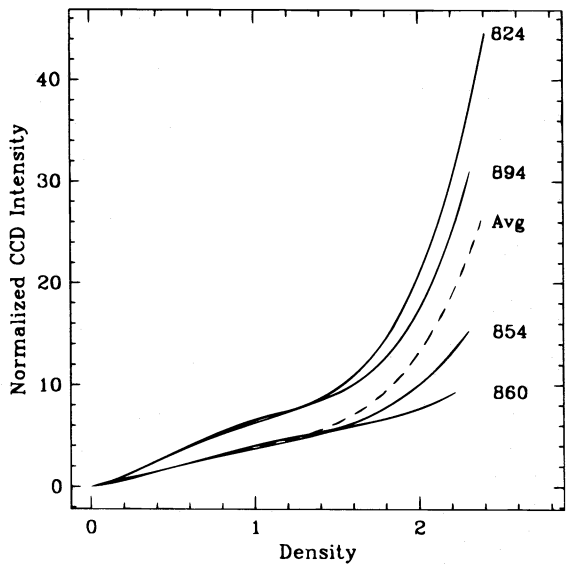

FIG. 2.—Plate-average characteristic curves for four representative UKST plates (*solid lines*), along with the overall average of the 13 well-calibrated plates (*dashed line*).

These transformation curves allow magnitudes to be estimated from the APM scans in the following manner. First, the background is measured as described above and subtracted from the scan. Second, the image is scaled into plate density units. Third, each pixel is transformed from a plate density value to a "normalized CCD B_J intensity" using the fourth-order polynomial fit to the applicable characteristic curve. Fourth, aperture photometry was performed on the transformed image in the same manner as for the CCD images to obtain a total intensity. Fifth, the total intensity was calibrated to a magnitude using an average B_J zero point for the relevant detector. Finally, to put all the galaxies on a common basis for comparisons, we converted the B_J magnitudes to B using the above color transformation equation and assuming $B-V = 0.53$, which is the median $B-V$ color of the 106 calibrator galaxies. The rms scatter in the $B-V$ colors of the calibrators is 0.21 mag, so the use of a fixed color term in the B_J-to-B transformation introduces a negligible additional uncertainty of 0.05 mag. Because the LAS and SAS lists were obtained from the same set of UKST plates, the same procedures were used for both lists. The method also yielded estimates of the half-light radius and central surface brightness, in the same manner as described above for the CCD images.

We note that our transformation uncertainties are larger than those obtained by Cawson et al. (1987) using this same procedure. First, they obtained CCD images of 17 galaxies to calibrate a single UKST plate, compared with our average number of four usable calibrators per plate. Second, their galaxies were bright, high-S/N ellipticals or early-type spirals with large numbers of pixels at flux levels well above the sky background. Most of the area of our LSB galaxies consists of pixels with net intensities only a few percent of the sky level. As a consequence, the characteristic curves of our galaxies are not as well determined, especially at the

bright end. Third, the Cawson et al. (1987) CCD data were obtained in one observing run, whereas our CCD images were taken on 19 different nights separated into eight observing runs distributed over a two year period. For all of these reasons, we were not able to duplicate their average photometric uncertainty of 0.1 mag. After accounting for the transformation uncertainties listed in Table 1, the zero-point uncertainties that result from using averages of zero points taken from many nights, and the usual internal measurement uncertainties, our number-weighted average photometric uncertainty is 0.20 mag per galaxy.

4. COMPLETENESS

As mentioned above, the scanning of the UKST plates was completed in two parts, the LAS list and the SAS list. Due to the timing of the plate scanning and the follow-up observations, and to the superior morphological information available for objects on the LAS list, all the follow-up observations were limited to the LAS list. However, the SAS list was developed using the same galaxy detection criteria as the LAS list, and from the same UKST plates. In evaluating the completeness of the survey, we will therefore consider the two lists together.

The digitized sections of UKST plates have high levels of background noise from different sources, including shot noise in the sky flux, emulsion response, emulsion grain size, chemical fog during development, and emulsion and chemical effects during photographic copying of the plates. Measurement of the background level and its uncertainty by the peak and width of the pixel histogram reveal that the 1 σ uncertainty is about 8 times the level predicted by a simple Poisson noise model assuming simple object-plus-sky photon counts; this difference is not surprising since much of the noise comes from sources other than photon counting. To complicate matters further, the noise is not random spatially; it is clumpy, or spatially correlated, with a correlation scale length (i.e., half-power point of the radial autocorrelation function) $\approx 3.2 \pm 0.3$ pixels. The correlation is caused by the finite spot size of the laser beam projected onto the plate (Gaussian core of ~ 10 μm FWHM) combined with the on-line 2×2 digital co-addition to form each output pixel.

To estimate the extent of this effect, and to understand the detection efficiency as a function of galaxy size and surface brightness, we created artificial APM scans of model galaxies with known structural parameters and passed these scans through the detection algorithm to determine the detection rate as a function of galaxy size and surface brightness. To simplify the analysis, we chose a face-on exponential profile for the model galaxies. This choice is reasonable for our survey, since most of our detected galaxies are fairly close to face-on (the median ellipticity as measured by simple moments analysis on the images is 0.23) and exhibit radial profiles in annular surface brightness versus radius plots that are well approximated by an exponential (see also Impey, Bothun, & Malin 1988; Bothun, Impey, & Malin 1991; McGaugh & Bothun 1994). Each model was therefore completely defined by two numbers, the central surface brightness [$\mu_B(0)$] and the exponential scale length ($r_{\rm scl}$). To simulate the effects of seeing, we convolved each model galaxy with a circular Gaussian of width comparable to that of the typical seeing disk on the APM scans. The seeing disk was found to have a size of $\approx 2''$ FWHM, as measured from the images of unsaturated stars.

Simulating the noisy background of the APM scans required matching both the overall noise level and the spatial correlation. We created images with a fixed background level and a large random noise component using a standard random number generator. This background-plus-noise image was then convolved with a circular Gaussian to simulate the clumpiness. The convolution also reduced the noise, so the noise level in the original artificial image was scaled up by the quadrature sum of the parameters of the convolving Gaussian function to give the desired noise level in the final, convolved image. Thorough testing confirmed that these convolved images were indistinguishable from the real APM scans in both background noise level and spatial correlation of the noise. Finally, the convolved noise image was added to the seeing-convolved model galaxy image to obtain the final image for analysis. This process ignores the additional Poisson noise component associated with flux from the galaxy (i.e., it assumes the galaxy itself is completely noiseless). This omission is harmless, however, as the background noise completely dominates the Poisson noise associated with the galaxy flux at the surface brightness levels of interest here.

For each pair of galaxy parameters [$\mu_B(0)$, $r_{\rm scl}$], 100 galaxy-plus-background–noise frames were created and passed through the detection algorithm, and a record was kept of the number of detections out of the 100 trials. Stepping through a grid of galaxy parameters allowed the development of a two-dimensional selection function, which gives the probability that a galaxy will be detected by the APM scan as a function of $\mu_B(0)$ and $r_{\rm scl}$. We then convolved the two-dimensional selection function with a one-dimensional Gaussian of $\sigma = 0.5$ mag arcsec^{-2} in the surface brightness dimension to account for the uncertainty in the average detection threshold used to develop the original function. The final selection function is shown in Figure 3. As anticipated, the surface defined by this function shows an effective completeness of 100% at central surface brightnesses brighter than $\mu_B(0) \approx 23.0$ mag arcsec^{-2}, and in the range of $\mu_B(0)$ where completeness is less than 100%, the completeness increases with increasing $r_{\rm scl}$.

The effectiveness of this completeness correction can be checked by applying the $\langle V/V_{\rm max}\rangle$ test of Schmidt (1968) and Felten (1976) to the combined (i.e., LAS list plus SAS list) sample of LSB galaxies. The APM detection process requires that detected galaxies have a minimum number of connected pixels at or above the detection threshold. This requirement is equivalent to a minimum angular diameter of 11.″5 for the case of an E0 or face-on spiral galaxy, cases which will give a minimum angular size for the given area. For an angular size limit $\theta_{\rm lim}$, $V/V_{\rm max} = (\theta_{\rm lim}/\theta_0)^3$, where θ_0 is the measured angular diameter of the galaxy at the limiting isophote. This calculation of $V/V_{\rm max}$ does not depend upon the intrinsic physical size of the galaxy, so there is no Malmquist-type bias. This simple calculation assumes no cosmological corrections in the relation between angular diameter and distance, but the median velocity of the LSB sample is only 7300 km s^{-1}, so the bias introduced is slight. There is also an implied apparent magnitude limit, based on the requirement that the pixels within the minimum area all at or above the detection threshold. Using the formalism of Davies (1993), the implied apparent magnitude limit for completeness here is ≈ 19 mag in B.

A simple unweighted average of the $V/V_{\rm max}$ values gives $\langle V/V_{\rm max}\rangle = 0.18 \pm 0.06$ (where the uncertainty is deter-

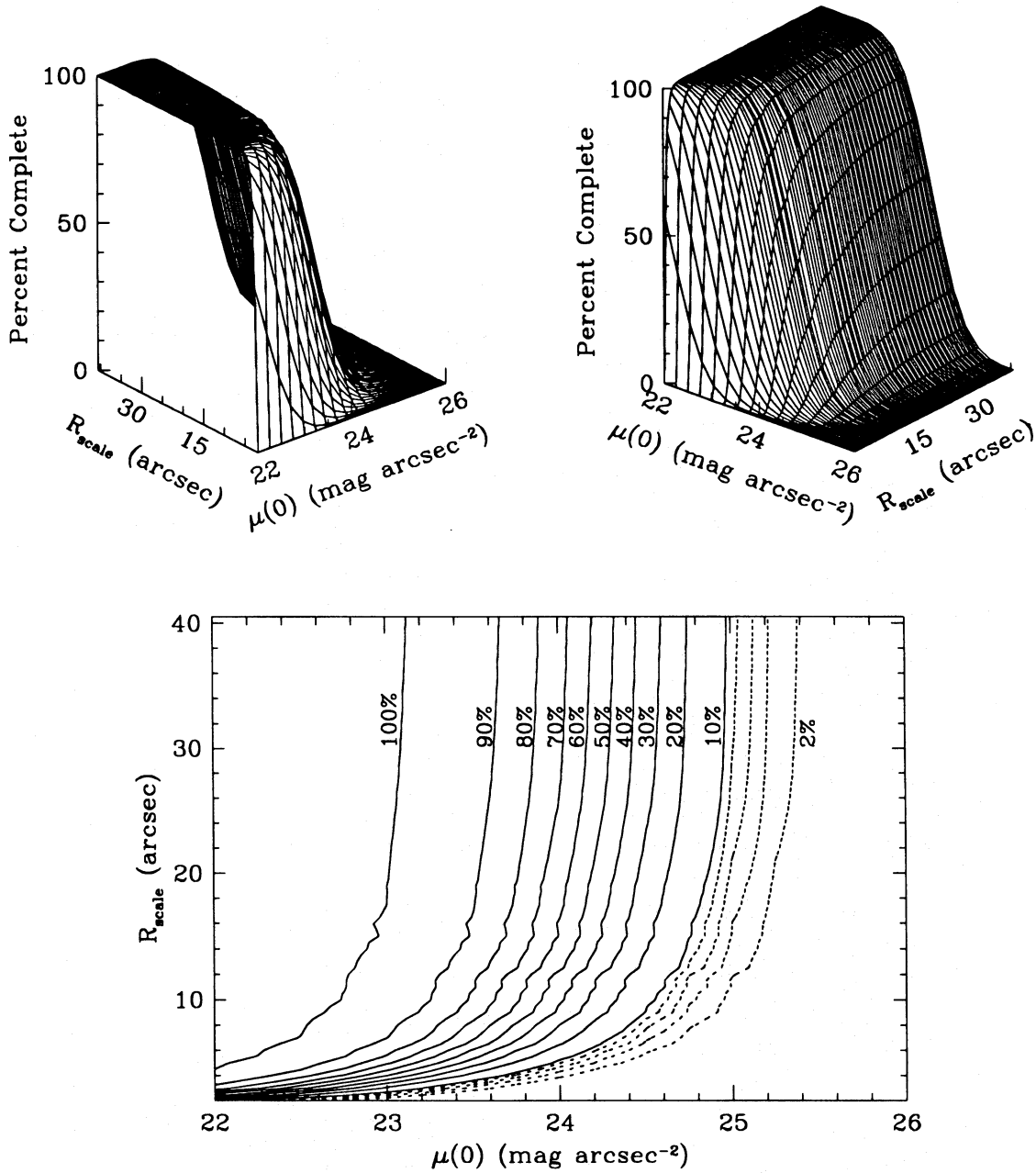

FIG. 3.—The selection function showing APM completeness as a function of galaxy $\mu_B(0)$ and r_{scl}. The upper panels are different perspective views of the surface, and the lower panel is a contour plot of the surface. In the lower panel, the dotted contours indicate a contour interval of 2% in completeness, running from 2% to 8%, and the solid contours indicate contour intervals of 10%, running from 10% to 100% completeness.

mined as $1/(12N)^{1/2}$, per Longair 1978), suggesting that the uncorrected sample is severely incomplete. For a weighted average V/V_{max}, where each galaxy is weighted by the inverse of the probability that it would be detected by the APM, the average rises to $\langle V/V_{max}\rangle = 0.44 \pm 0.06$. The selection function depicted in Figure 3 therefore substantially accounts for the incompleteness in the survey. The corrections become very large for $\mu_B(0) > 24.5$ mag arcsec^{-2} and $r_{scl} < 5''$, or for $\mu_B(0) > 25.5$ mag arcsec^{-2} at any scale length, so to be conservative we claim the corrected survey is essentially complete to the values of $\mu_B(0)$ and r_{scl} that define the 10% completeness contour in Figure 3. The "knee" of that contour is at $\mu_B(0) \approx 24.5$ mag arcsec^{-2} and $r_{scl} \approx 10''$, so we adopt those numbers as the characteristic completeness limits of the survey.

5. IMPLICATIONS

A debate has continued for some time over the question of whether disk galaxies have a preferred value of central surface brightness. Freeman (1970) first claimed the preferred value is $\mu_B(0) = 21.65 \pm 0.3$ mag arcsec^{-2} for 28 galaxies drawn from a sample of 36 NGC objects with published surface photometry. More recently, van der Kruit (1987) obtained a similar result [$\mu_{B_J}(0) = 21.8 \pm 0.6$ mag arcsec^{-2}] from a carefully chosen sample of 40 face-on UGC galaxies.

On the other hand, Disney (1976) argued that selection effects in photographic surveys could account for the observation of similar central surface brightnesses, and that the limiting isophote of the Palomar Observatory Sky

Survey would quantitatively explain the preferred value of 21.65 mag arcsec^{-2}. At a given galaxy luminosity, galaxies of both low and high central surface brightness would tend to be excluded from galaxy surveys: high surface brightness (HSB) galaxies because they are mistaken for stars, and LSB galaxies because they do not have a large enough angular size at the limiting isophote to be cataloged. Allen & Shu (1979) agreed that such selection effects could cause LSB galaxies to be missed but maintained that the available data do not indicate a bias against finding HSB galaxies. Disney & Phillipps (1983) derived a method of estimating the maximum volume over which a spiral galaxy with a given central surface brightness would be visible (which they called the "visibility" of the galaxy) using the detection limits of the survey in question; this visibility, as a function of surface brightness, can then be used to obtain the true surface brightness distribution from the observed one.

The present survey offers a unique opportunity to test the contentions on both sides of this argument. We have developed a sample of galaxies that is complete within well-defined limits of central surface brightness and angular size, and is therefore free of any biases that may be present in existing catalogs such as the NGC or the UGC. The catalog of LSB galaxies described in § 2 will of course not illustrate the true distribution of central surface brightnesses, because most of the galaxies with $\mu(0) \lesssim 22$ mag arcsec^{-2} were deliberately excluded. It is possible, however, to find the true distribution using the full information obtained in the course of the machine scanning that developed the LSB catalog. Specifically, we have preserved the complete list of objects identified by the APM machine as having the required number of connected pixels above the detection threshold, i.e., before the exclusion of the HSB objects. We have reviewed this list for one of the UKST fields listed in Table 1 (field 826) to eliminate the obvious plate flaws, overlapping stars, and other interlopers (about 15% of the total number of "objects" identified), leaving a final list of 1595 galaxies detected in the 5°.8 × 5°.8 field.

Figure 4 shows the distribution of central surface brightnesses among these 1595 galaxies. These central surface brightnesses were determined by the APM image identification routine via extrapolation from the areal profile, as described in § 2. Although these values were not determined in the same way as the central surface brightnesses used to obtain the selection function of § 4, the measurements are quite consistent between the two methods. The difference $\mu_{\rm aper} - \mu_{\rm extr} = 0.3 \pm 0.8$ (where $\mu_{\rm aper}$ is the central surface brightness for the LSB galaxies described in § 3 and $\mu_{\rm extr}$ is the central surface brightness obtained from extrapolation of the APM areal profile) is small and follows a roughly Gaussian distribution, indicating that there is no major systematic difference between the two sets. This comparability of the $\mu(0)$ values allows the direct application of the selection function shown in Figure 3 to the full set of 1595 galaxies, thus correcting for the incompleteness at faint $\mu(0)$ and small $r_{\rm scl}$ caused by the search procedure itself. The distribution for field 826 after correction for this incompleteness is also shown in Figure 4.

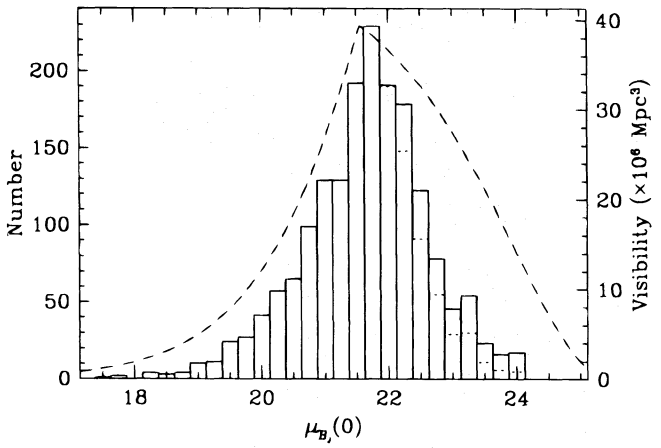

FIG. 4.—Observed distribution of central surface brightnesses for UKST field 826. The dotted histogram shows the distribution before correction by the APM selection function, and the solid histogram shows the distribution after correction. The dashed curve shows the visibility function described in the text, and the vertical axis on the right shows the units and scaling of the visibility function.

Figure 4 does not show the true distribution of central surface brightnesses in field 826, but only the observed distribution corrected for the known incompleteness in the mechanical survey method. As Disney & Phillipps (1983) illustrated, the visibility function (i.e., that gives the maximum volume over which a galaxy can be seen as a function of the galaxy's central surface brightness) for a given survey is uniquely determined by that survey's limiting parameters: the limiting apparent magnitude $m_{\rm lim}$, the limiting angular radius $\theta_{\rm lim}$, and the surface brightness detection limit $\mu_{\rm lim}$. We have computed the visibility function for the APM machine search of field 826 using the actual parameters of the search, determined using the photometric calibrations for that field: $\mu_{\rm lim} = 25.7 B_J$ mag arcsec^{-2}, $\theta_{\rm lim} = 5''.7$, and $m_{\rm lim} = 18.8 B_J$ mag. Because these galaxies were selected solely on the basis of a number of connected pixels above a threshold level, this "limiting magnitude" is derived from the limiting angular size and the detection threshold simply as $m_{\rm lim} = \mu_{\rm lim} - 2.5 \log (2e\pi\theta^2_{\rm lim})$. The peak of the visibility function coincides with the peak in the observed distribution, and the overall shape of the visibility function roughly matches the shape of the distribution. However, the visibility function is somewhat wider than the data distribution.

The solid squares in Figure 5 show the log of the observed distribution of central surface brightnesses in field 826 divided by the visibility function for that field and normalized to unity at $\mu_{B_J}(0) = 21.75$ mag arcsec^{-2}, thus giving the relative space density of galaxies as a function of $\mu(0)$. The error bars reflect counting statistics and the effects of the corrections. The distribution rises slowly over the range $18 < \mu(0) < 22$ and then declines over the range $22 < \mu(0) < 23.75$. There is still a peak at $\mu(0) = 22$ mag arcsec^{-2}, very close to the peak values observed by Freeman (1970) and van der Kruit (1987). However, the distribution here has a FWHM of about 3 mag arcsec^{-2}, much broader than those observed by Freeman (1970) and van der Kruit (1987). Figure 5 also supports the contention of Allen & Shu (1979) that selection biases cannot fully account for the relative dearth of HSB galaxies. Further support on this point comes from the efforts of Disney (1994, private communication) and coworkers, who have used machine scanning and automated classification algorithms to search for putative HSB galaxies belonging to the Fornax cluster. Although a few previously unknown HSB cluster members were found, there was clear evidence that a large hidden HSB population is not present in the Fornax cluster. The crosses in Figure 5 show the values for the

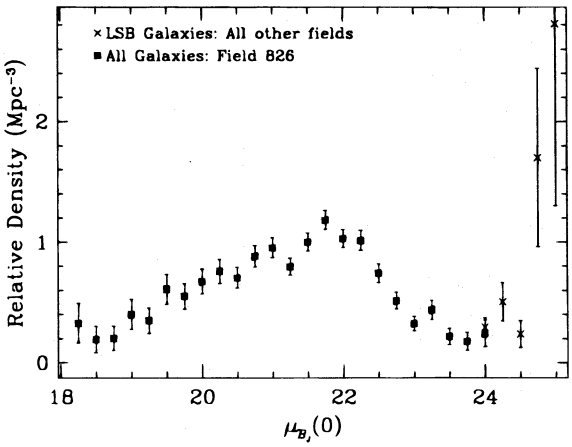

FIG. 5.—Distributions of central surface brightnesses in field 826 (*solid squares*), after correction by the visibility function described in the text, and among the LSB galaxies from all other fields (*crosses*), also corrected by appropriate visibility functions. The visibility function has units of volume, so these distributions have units of number density, but they are arbitrarily normalized to unity at $\mu(0) = 21.75$.

density of LSB galaxies determined from the remaining 23 fields in our survey, normalized in the same manner as the densities for field 826. These points are included to reduce the statistical errors at the LSB end of the distribution, and they show that the density of galaxies over the range $23 < \mu(0) < 25$ is at least constant out to the limits of this survey. The density appears to increase at the very faintest surface brightness levels of our survey, but this apparent increase should not be taken too seriously, since the uncertainties on these last two points are quite large due to the large corrections for visibility and survey incompleteness.

This distribution in field 826 is in general agreement with the findings of Phillipps et al. (1987), who performed a similar APM-based search of the Fornax cluster. They found a distribution peaked at about $\mu(0) = 21.75$, with a FWHM of about 2 mag arcsec^{-2}. They also found that the cluster distribution had a long tail at low surface brightnesses, consistent with constant number density from $23 < \mu(0) < 24.5$ at a level of about $\frac{1}{4} - \frac{1}{5}$ of the peak value. Considering our field 826 and all-fields distributions together, the result found here resembles their distribution for the Fornax cluster. The densities found here also decline for central surface brightnesses fainter than $\mu_B \sim 22$, and they also seem to reach a plateau at about $\frac{1}{4} - \frac{1}{3}$ the peak level in the range $23 < \mu(0) < 25$.

6. CONCLUSIONS

We have described the process of identifying LSB galaxies from the UKST survey plates using a combination of APM and visual searches. We have measured the apparent magnitudes of the identified LSB galaxies with a typical uncertainty of $\sigma = 0.20$ mag in B, using pixel-to-pixel transformations calibrated by CCD observations of 106 of the LSB galaxies. Through simulations of the APM detection process, we have developed a selection function for the APM survey that describes the probability that an LSB galaxy will be included in our catalog as a function of the galaxy's central surface brightness and scale length, and we have demonstrated that this objectively determined selection function substantially corrects for the incompleteness in the catalog. Finally, we have obtained the complete distribution of central surface brightnesses from one UKST survey field and corrected that distribution for the visibility described by Disney & Phillipps (1983). The resulting distribution is very broad, with a peak at $\mu_B(0) \approx 22$ mag arcsec^{-2}, a decline over the range $22 \leq \mu_B(0) \leq 23.75$, and a flat or increasing level for $\mu_B(0) \geq 23.75$. This distribution is much broader than those described by Freeman (1970) and van der Kruit (1987).

We thank Greg Bothun and Stacy McGaugh for many helpful and stimulating discussions. We are grateful for the expert assistance from the staff at the Steward Observatory Kitt Peak Station during the many observing runs carried out in connection with our survey of LSB galaxies. This research made use of NASA's Astrophysics Data System version 4.0. This research was supported in part by National Science Foundation grant AST 90-03158. D. S. was supported by a National Science Foundation Graduate Research Fellowship.

REFERENCES

Allen, R. J., & Shu, F. H. 1979, ApJ, 227, 67
Blair, M., & Gilmore, G. 1982, PASP, 94, 742
Bothun, G. D., Impey, C. D., & Malin, D. F. 1991, ApJ, 376, 404
Bothun, G. D., Impey, C. D., Malin, D. F., & Mould, J. R. 1987, AJ, 94, 23
Burstein, D., & Heiles, C. 1982, AJ, 87, 1165
Cawson, M. G. M., Kibblewhite, E. J., Disney, M. J., & Phillipps, S. 1987, MNRAS, 224, 557
Christian, C. A., Adams, M., Barnes, J. V., Butcher, H., Hayes, D. S., Mould, J. R., & Siegel, M. 1985, PASP, 97, 363
Coleman, G. D., Wu, C.-C., & Weedman, D. W. 1980, ApJS, 43, 393
Davies, J. I. 1993, in The Environment and Evolution of Galaxies, ed. J. M. Shull & H. A. Thronson, Jr. (Dordrecht: Kluwer), 105
Davies, J. I., Disney, M. J., Phillipps, S., Boyle, B. J., & Couch, W. J. 1994, MNRAS, 269, 349
Disney, M., & Phillipps, S. 1983, MNRAS, 205, 1253
Disney, M. J. 1976, Nature, 263, 573
Felten, J. E. 1976, ApJ, 207, 700
Freeman, K. C. 1970, ApJ, 160, 811
Impey, C. D., Bothun, G. D., & Malin, D. F. 1988, ApJ, 330, 634
Impey, C. D., Sprayberry, D., Irwin, M. J., & Bothun, G. D. 1996, ApJS, in press
Irwin, M. J., Davies, J. I., Disney, M. J., & Phillipps, S. 1990, MNRAS, 245, 289
Kibblewhite, E. J., Bridgeland, M. T., Bunclark, P. S., & Irwin, M. J. 1984, in NASA Conf. Pub. No. 2317, Astronomical Microdensitometry Conference, ed. D. A. Klinglesmith (Washington, D. C.: NASA), 277
Longair, M. S. 1978, in Observational Cosmology: Eighth Advanced Course of the Swiss Society of Astronomy and Astrophysics (Sauverny: Geneva Observatory), 125
McGaugh, S. S., & Bothun, G. D. 1994, AJ, 107, 530
Odewahn, S. C., Bryja, C., & Humphreys, R. M. 1992, PASP, 104, 553
Phillipps, S., Disney, M. J., Kibblewhite, E. J., & Cawson, M. G. M. 1987, MNRAS, 229, 505
Schmidt, M. 1968, ApJ, 151, 393
Schombert, J. M., & Bothun, G. D. 1988, AJ, 95, 1389
Schombert, J. M., Bothun, G. D., Schneider, S. E., & McGaugh, S. S. 1992, AJ, 103, 1107
Sprayberry, D., Impey, C. D., Irwin, M. J., McMahon, R. G., & Bothun, G. D. 1993, ApJ, 417, 114
van der Kruit, P. C. 1987, A&A, 173, 59